Updated search for the standard model Higgs boson in events with jets and missing transverse energy using the full CDF data set

T. Aaltonen,[21] S. Amerio,[40] D. Amidei,[32] A. Anastassov[x],[15] A. Annovi,[17] J. Antos,[12] G. Apollinari,[15] J.A. Appel,[15] T. Arisawa,[53] A. Artikov,[13] J. Asaadi,[48] W. Ashmanskas,[15] B. Auerbach,[2] A. Aurisano,[48] F. Azfar,[39] W. Badgett,[15] T. Bae,[25] A. Barbaro-Galtieri,[26] V.E. Barnes,[44] B.A. Barnett,[23] P. Barria[hh],[42] P. Bartos,[12] M. Bauce[ff],[40] F. Bedeschi,[42] S. Behari,[15] G. Bellettini[gg],[42] J. Bellinger,[55] D. Benjamin,[14] A. Beretvas,[15] A. Bhatti,[46] K.R. Bland,[5] B. Blumenfeld,[23] A. Bocci,[14] A. Bodek,[45] D. Bortoletto,[44] J. Boudreau,[43] A. Boveia,[11] L. Brigliadori[ee],[6] C. Bromberg,[33] E. Brucken,[21] J. Budagov,[13] H.S. Budd,[45] K. Burkett,[15] G. Busetto[ff],[40] P. Bussey,[19] P. Butti[gg],[42] A. Buzatu,[19] A. Calamba,[10] S. Camarda,[4] M. Campanelli,[28] F. Canelli[oo],[11,15] B. Carls,[22] D. Carlsmith,[55] R. Carosi,[42] S. Carrillo[m],[16] B. Casal[k],[9] M. Casarsa,[49] A. Castro[ee],[6] P. Catastini,[20] D. Cauz,[49] V. Cavaliere,[22] M. Cavalli-Sforza,[4] A. Cerri[f],[26] L. Cerrito[s],[28] Y.C. Chen,[1] M. Chertok,[7] G. Chiarelli,[42] G. Chlachidze,[15] K. Cho,[25] D. Chokheli,[13] M.A. Ciocci[hh],[42] A. Clark,[18] C. Clarke,[54] M.E. Convery,[15] J. Conway,[7] M .Corbo,[15] M. Cordelli,[17] C.A. Cox,[7] D.J. Cox,[7] M. Cremonesi,[42] D. Cruz,[48] J. Cuevas[z],[9] R. Culbertson,[15] N. d'Ascenzo[w],[15] M. Datta[qq],[15] P. De Barbaro,[45] L. Demortier,[46] M. Deninno,[6] F. Devoto,[21] M. d'Errico[ff],[40] A. Di Canto[gg],[42] B. Di Ruzza[q],[15] J.R. Dittmann,[5] M. D'Onofrio,[27] S. Donati[gg],[42] M. Dorigo[nn],[49] A. Driutti,[49] K. Ebina,[53] R. Edgar,[32] A. Elagin,[48] R. Erbacher,[7] S. Errede,[22] B. Esham,[22] R. Eusebi,[48] S. Farrington,[39] J.P. Fernández Ramos,[29] R. Field,[16] G. Flanagan[u],[15] R. Forrest,[7] M. Franklin,[20] J.C. Freeman,[15] H. Frisch,[11] Y. Funakoshi,[53] A.F. Garfinkel,[44] P. Garosi[hh],[42] H. Gerberich,[22] E. Gerchtein,[15] S. Giagu,[47] V. Giakoumopoulou,[3] K. Gibson,[43] C.M. Ginsburg,[15] N. Giokaris,[3] P. Giromini,[17] G. Giurgiu,[23] V. Glagolev,[13] D. Glenzinski,[15] M. Gold,[35] D. Goldin,[48] A. Golossanov,[15] G. Gomez,[9] G. Gomez-Ceballos,[30] M. Goncharov,[30] O. González López,[29] I. Gorelov,[35] A.T. Goshaw,[14] K. Goulianos,[46] E. Gramellini,[6] S. Grinstein,[4] C. Grosso-Pilcher,[11] R.C. Group[52],[15] J. Guimaraes da Costa,[20] S.R. Hahn,[15] J.Y. Han,[45] F. Happacher,[17] K. Hara,[50] M. Hare,[51] R.F. Harr,[54] T. Harrington-Taber[n],[15] K. Hatakeyama,[5] C. Hays,[39] J. Heinrich,[41] M. Herndon,[55] A. Hocker,[15] Z. Hong,[48] W. Hopkins[g],[15] S. Hou,[1] R.E. Hughes,[36] U. Husemann,[56] J. Huston,[33] G. Introzzi[mm],[42] M. Iori[jj],[47] A. Ivanov[p],[7] E. James,[15] D. Jang,[10] B. Jayatilaka,[15] E.J. Jeon,[25] S. Jindariani,[15] M. Jones,[44] K.K. Joo,[25] S.Y. Jun,[10] T.R. Junk,[15] M. Kambeitz,[24] T. Kamon[25],[48] P.E. Karchin,[54] A. Kasmi,[5] Y. Kato[o],[38] W. Ketchum[rr],[11] J. Keung,[41] B. Kilminster[oo],[15] D.H. Kim,[25] H.S. Kim,[25] J.E. Kim,[25] M.J. Kim,[17] S.B. Kim,[25] S.H. Kim,[50] Y.K. Kim,[11] Y.J. Kim,[25] N. Kimura,[53] M. Kirby,[15] K. Knoepfel,[15] K. Kondo*,[53] D.J. Kong,[25] J. Konigsberg,[16] A.V. Kotwal,[14] M. Kreps,[24] J. Kroll,[41] M. Kruse,[14] T. Kuhr,[24] M. Kurata,[50] A.T. Laasanen,[44] S. Lammel,[15] M. Lancaster,[28] K. Lannon[y],[36] G. Latino[hh],[42] H.S. Lee,[25] J.S. Lee,[25] S. Leo,[42] S. Leone,[42] J.D. Lewis,[15] A. Limosani[t],[14] E. Lipeles,[41] H. Liu,[52] Q. Liu,[44] T. Liu,[15] S. Lockwitz,[56] A. Loginov,[56] D. Lucchesi[ff],[40] J. Lueck,[24] P. Lujan,[26] P. Lukens,[15] G. Lungu,[46] J. Lys,[26] R. Lysak[e],[12] R. Madrak,[15] P. Maestro[hh],[42] S. Malik,[46] G. Manca[a],[27] A. Manousakis-Katsikakis,[3] F. Margaroli,[47] P. Marino[ii],[42] M. Martínez,[4] K. Matera,[22] M.E. Mattson,[54] A. Mazzacane,[15] P. Mazzanti,[6] R. McNulty[j],[27] A. Mehta,[27] P. Mehtala,[21] C. Mesropian,[46] T. Miao,[15] D. Mietlicki,[32] A. Mitra,[1] H. Miyake,[50] S. Moed,[15] N. Moggi,[6] C.S. Moon[aa],[15] R. Moore[pp],[15] M.J. Morello[ii],[42] A. Mukherjee,[15] Th. Muller,[24] P. Murat,[15] M. Mussini[ee],[6] J. Nachtman[n],[15] Y. Nagai,[50] J. Naganoma,[53] I. Nakano,[37] A. Napier,[51] J. Nett,[48] C. Neu,[52] T. Nigmanov,[43] L. Nodulman,[2] S.Y. Noh,[25] O. Norniella,[22] L. Oakes,[39] S.H. Oh,[14] Y.D. Oh,[25] I. Oksuzian,[52] T. Okusawa,[38] R. Orava,[21] L. Ortolan,[4] C. Pagliarone,[49] E. Palencia[f],[9] P. Palni,[35] V. Papadimitriou,[15] W. Parker,[55] G. Pauletta[kk],[49] M. Paulini,[10] C. Paus,[30] T.J. Phillips,[14] G. Piacentino,[42] E. Pianori,[41] J. Pilot,[36] K. Pitts,[22] C. Plager,[8] L. Pondrom,[55] S. Poprocki[g],[15] K. Potamianos,[26] F. Prokoshin[cc],[13] A. Pranko,[26] F. Ptohos[h],[17] G. Punzi[gg],[42] N. Ranjan,[44] I. Redondo Fernández,[29] P. Renton,[39] M. Rescigno,[47] T. Riddick,[28] F. Rimondi*,[6] L. Ristori[42],[15] A. Robson,[19] T. Rodriguez,[41] S. Rolli[i],[51] M. Ronzani[gg],[42] R. Roser,[15] J.L. Rosner,[11] F. Ruffini[hh],[42] A. Ruiz,[9] J. Russ,[10] V. Rusu,[15] A. Safonov,[48] W.K. Sakumoto,[45] Y. Sakurai,[53] L. Santi[kk],[49] K. Sato,[50] V. Saveliev[w],[15] A. Savoy-Navarro[aa],[15] P. Schlabach,[15] E.E. Schmidt,[15] T. Schwarz,[32] L. Scodellaro,[9] F. Scuri,[42] S. Seidel,[35] Y. Seiya,[38] A. Semenov,[13] F. Sforza[gg],[42] S.Z. Shalhout,[7] T. Shears,[27] P.F. Shepard,[43] M. Shimojima[v],[50] M. Shochet,[11] I. Shreyber-Tecker,[34] A. Simonenko,[13] P. Sinervo,[31] K. Sliwa,[51] J.R. Smith,[7] F.D. Snider,[15] V. Sorin,[4] H. Song,[43] M. Stancari,[15] R. St. Denis,[19] B. Stelzer,[31] O. Stelzer-Chilton,[31] D. Stentz[x],[15] J. Strologas,[35] Y. Sudo,[50] A. Sukhanov,[15] I. Suslov,[13] K. Takemasa,[50] Y. Takeuchi,[50] J. Tang,[11] M. Tecchio,[32] P.K. Teng,[1] J. Thom[g],[15] E. Thomson,[41] V. Thukral,[48] D. Toback,[48] S. Tokar,[12] K. Tollefson,[33] T. Tomura,[50] D. Tonelli[f],[15] S. Torre,[17] D. Torretta,[15] P. Totaro,[40] M. Trovato[ii],[42] F. Ukegawa,[50] S. Uozumi,[25] F. Vázquez[m],[16] G. Velev,[15] C. Vellidis,[15] C. Vernieri[ii],[42] M. Vidal,[44] R. Vilar,[9] J. Vizán[ll],[9] M. Vogel,[35] G. Volpi,[17] P. Wagner,[41] R. Wallny,[8] S.M. Wang,[1] A. Warburton,[31] D. Waters,[28] W.C. Wester III,[15] D. Whiteson[b],[41] A.B. Wicklund,[2] S. Wilbur,[11] H.H. Williams,[41]

J.S. Wilson,[32] P. Wilson,[15] B.L. Winer,[36] P. Wittich[g],[15] S. Wolbers,[15] H. Wolfe,[36] T. Wright,[32] X. Wu,[18] Z. Wu,[5] K. Yamamoto,[38] D. Yamato,[38] T. Yang,[15] U.K. Yang[r],[11] Y.C. Yang,[25] W.-M. Yao,[26] G.P. Yeh,[15] K. Yi[n],[15] J. Yoh,[15] K. Yorita,[53] T. Yoshida[l],[38] G.B. Yu,[14] I. Yu,[25] A.M. Zanetti,[49] Y. Zeng,[14] C. Zhou,[14] and S. Zucchelli[ee6]

(CDF Collaboration[†])

[1]*Institute of Physics, Academia Sinica, Taipei, Taiwan 11529, Republic of China*
[2]*Argonne National Laboratory, Argonne, Illinois 60439, USA*
[3]*University of Athens, 157 71 Athens, Greece*
[4]*Institut de Fisica d'Altes Energies, ICREA, Universitat Autonoma de Barcelona, E-08193, Bellaterra (Barcelona), Spain*
[5]*Baylor University, Waco, Texas 76798, USA*
[6]*Istituto Nazionale di Fisica Nucleare Bologna, [ee] University of Bologna, I-40127 Bologna, Italy*
[7]*University of California, Davis, Davis, California 95616, USA*
[8]*University of California, Los Angeles, Los Angeles, California 90024, USA*
[9]*Instituto de Fisica de Cantabria, CSIC-University of Cantabria, 39005 Santander, Spain*
[10]*Carnegie Mellon University, Pittsburgh, Pennsylvania 15213, USA*
[11]*Enrico Fermi Institute, University of Chicago, Chicago, Illinois 60637, USA*
[12]*Comenius University, 842 48 Bratislava, Slovakia; Institute of Experimental Physics, 040 01 Kosice, Slovakia*
[13]*Joint Institute for Nuclear Research, RU-141980 Dubna, Russia*
[14]*Duke University, Durham, North Carolina 27708, USA*
[15]*Fermi National Accelerator Laboratory, Batavia, Illinois 60510, USA*
[16]*University of Florida, Gainesville, Florida 32611, USA*
[17]*Laboratori Nazionali di Frascati, Istituto Nazionale di Fisica Nucleare, I-00044 Frascati, Italy*
[18]*University of Geneva, CH-1211 Geneva 4, Switzerland*
[19]*Glasgow University, Glasgow G12 8QQ, United Kingdom*
[20]*Harvard University, Cambridge, Massachusetts 02138, USA*
[21]*Division of High Energy Physics, Department of Physics,*
University of Helsinki and Helsinki Institute of Physics, FIN-00014, Helsinki, Finland
[22]*University of Illinois, Urbana, Illinois 61801, USA*
[23]*The Johns Hopkins University, Baltimore, Maryland 21218, USA*
[24]*Institut für Experimentelle Kernphysik, Karlsruhe Institute of Technology, D-76131 Karlsruhe, Germany*
[25]*Center for High Energy Physics: Kyungpook National University,*
Daegu 702-701, Korea; Seoul National University, Seoul 151-742,
Korea; Sungkyunkwan University, Suwon 440-746,
Korea; Korea Institute of Science and Technology Information,
Daejeon 305-806, Korea; Chonnam National University,
Gwangju 500-757, Korea; Chonbuk National University, Jeonju 561-756,
Korea; Ewha Womans University, Seoul, 120-750, Korea
[26]*Ernest Orlando Lawrence Berkeley National Laboratory, Berkeley, California 94720, USA*
[27]*University of Liverpool, Liverpool L69 7ZE, United Kingdom*
[28]*University College London, London WC1E 6BT, United Kingdom*
[29]*Centro de Investigaciones Energeticas Medioambientales y Tecnologicas, E-28040 Madrid, Spain*
[30]*Massachusetts Institute of Technology, Cambridge, Massachusetts 02139, USA*
[31]*Institute of Particle Physics: McGill University, Montréal, Québec H3A 2T8,*
Canada; Simon Fraser University, Burnaby, British Columbia V5A 1S6,
Canada; University of Toronto, Toronto, Ontario M5S 1A7,
Canada; and TRIUMF, Vancouver, British Columbia V6T 2A3, Canada
[32]*University of Michigan, Ann Arbor, Michigan 48109, USA*
[33]*Michigan State University, East Lansing, Michigan 48824, USA*
[34]*Institution for Theoretical and Experimental Physics, ITEP, Moscow 117259, Russia*
[35]*University of New Mexico, Albuquerque, New Mexico 87131, USA*
[36]*The Ohio State University, Columbus, Ohio 43210, USA*
[37]*Okayama University, Okayama 700-8530, Japan*
[38]*Osaka City University, Osaka 588, Japan*
[39]*University of Oxford, Oxford OX1 3RH, United Kingdom*
[40]*Istituto Nazionale di Fisica Nucleare, Sezione di Padova-Trento, [ff] University of Padova, I-35131 Padova, Italy*
[41]*University of Pennsylvania, Philadelphia, Pennsylvania 19104, USA*
[42]*Istituto Nazionale di Fisica Nucleare Pisa, [gg] University of Pisa,*
[hh] University of Siena and [ii] Scuola Normale Superiore, I-56127 Pisa,
Italy, [mm] INFN Pavia and University of Pavia, I-27100 Pavia, Italy
[43]*University of Pittsburgh, Pittsburgh, Pennsylvania 15260, USA*
[44]*Purdue University, West Lafayette, Indiana 47907, USA*
[45]*University of Rochester, Rochester, New York 14627, USA*
[46]*The Rockefeller University, New York, New York 10065, USA*

[47]Istituto Nazionale di Fisica Nucleare, Sezione di Roma 1,
[jj]Sapienza Università di Roma, I-00185 Roma, Italy
[48]Texas A&M University, College Station, Texas 77843, USA
[49]Istituto Nazionale di Fisica Nucleare Trieste/Udine; [nn]University of Trieste,
I-34127 Trieste, Italy; [kk]University of Udine, I-33100 Udine, Italy
[50]University of Tsukuba, Tsukuba, Ibaraki 305, Japan
[51]Tufts University, Medford, Massachusetts 02155, USA
[52]University of Virginia, Charlottesville, Virginia 22906, USA
[53]Waseda University, Tokyo 169, Japan
[54]Wayne State University, Detroit, Michigan 48201, USA
[55]University of Wisconsin, Madison, Wisconsin 53706, USA
[56]Yale University, New Haven, Connecticut 06520, USA

(Dated: January 21, 2013)

We present an updated search for the Higgs boson produced in association with a vector boson in the final state with missing transverse energy and two jets. We use the full CDF data set corresponding to an integrated luminosity of 9.45 fb^{-1} at a proton-antiproton center-of-mass energy of $\sqrt{s} = 1.96$ TeV. New to this analysis is the inclusion of a b-jet identification algorithm specifically optimized for $H \to b\bar{b}$ searches. Across the Higgs boson mass range $90 \leq m_H \leq 150$ GeV/c^2, the expected 95% credibility level upper limits on the VH production cross section times the $H \to b\bar{b}$ branching fraction are improved by an average of 14% relative to the previous analysis. At a Higgs boson mass of 125 GeV/c^2, the observed (expected) limit is 3.06 (3.33) times the standard model prediction, corresponding to one of the most sensitive searches to date in this final state.

PACS numbers: 13.85.Rm, 14.80.Bn

I. INTRODUCTION

In the standard model of particle physics (SM) [1], the mechanism of electroweak symmetry breaking generates a massive scalar boson called the Higgs boson (H) [2]. Over the last few decades there has been an intensive effort to uncover experimental evidence of the existence of the Higgs boson. Recently, the CMS and ATLAS collaborations reported the observation of a new boson with a mass of approximately 125 GeV/c^2 [3]. While the production and decay of this particle are consistent with expectations for the SM Higgs boson, many of its properties have yet to be established. In particular, the relative coupling strengths of this boson to quarks, leptons, and other bosons are important in understanding whether it is the SM Higgs boson or another state. While the sensitivities of the CMS and ATLAS analyses were primarily influenced by decays of this particle into Z bosons, W bosons, and photons, the sensitivity of the low-mass Higgs boson analyses of the CDF and D0 collaborations is largely from decays to pairs of b quarks. Recent results from CDF and D0 show evidence of an excess of events consistent with a 125 GeV/c^2 SM Higgs boson decaying to b quarks [4]. However, it is not yet known if this excess can be attributed to the same particle observed by the ATLAS and CMS collaborations and further investigation is warranted.

In the SM, the dominant decay channel for a low-mass Higgs boson ($m_H \leq 135$ GeV/c^2) is to the $b\bar{b}$ final state. At the Tevatron, pairs of b quarks are produced via the strong interaction ("QCD multijet" background) with a cross section much larger than that predicted for Higgs boson production followed by $H \to b\bar{b}$ decay. Searching for direct Higgs boson production is, therefore, very

*Deceased
†With visitors from [a]Istituto Nazionale di Fisica Nucleare, Sezione di Cagliari, 09042 Monserrato (Cagliari), Italy, [b]University of California Irvine, Irvine, CA 92697, USA, [c]University of California Santa Barbara, Santa Barbara, CA 93106, USA, [d]University of California Santa Cruz, Santa Cruz, CA 95064, USA, [e]Institute of Physics, Academy of Sciences of the Czech Republic, 182 21, Czech Republic, [f]CERN, CH-1211 Geneva, Switzerland, [g]Cornell University, Ithaca, NY 14853, USA, [h]University of Cyprus, Nicosia CY-1678, Cyprus, [i]Office of Science, U.S. Department of Energy, Washington, DC 20585, USA, [j]University College Dublin, Dublin 4, Ireland, [k]ETH, 8092 Zürich, Switzerland, [l]University of Fukui, Fukui City, Fukui Prefecture, Japan 910-0017, [m]Universidad Iberoamericana, Lomas de Santa Fe, México, C.P. 01219, Distrito Federal, [n]University of Iowa, Iowa City, IA 52242, USA, [o]Kinki University, Higashi-Osaka City, Japan 577-8502, [p]Kansas State University, Manhattan, KS 66506, USA, [q]Brookhaven National Laboratory, Upton, NY 11973, USA, [r]University of Manchester, Manchester M13 9PL, United Kingdom, [s]Queen Mary, University of London, London, E1 4NS, United Kingdom, [t]University of Melbourne, Victoria 3010, Australia, [u]Muons, Inc., Batavia, IL 60510, USA, [v]Nagasaki Institute of Applied Science, Nagasaki 851-0193, Japan, [w]National Research Nuclear University, Moscow 115409, Russia, [x]Northwestern University, Evanston, IL 60208, USA, [y]University of Notre Dame, Notre Dame, IN 46556, USA, [z]Universidad de Oviedo, E-33007 Oviedo, Spain, [aa]CNRS-IN2P3, Paris, F-75205 France, [bb]Texas Tech University, Lubbock, TX 79609, USA, [cc]Universidad Tecnica Federico Santa Maria, 110v Valparaiso, Chile, [dd]Yarmouk University, Irbid 211-63, Jordan, [ll]Universite catholique de Louvain, 1348 Louvain-La-Neuve, Belgium, [oo]University of Zürich, 8006 Zürich, Switzerland, [pp]Massachusetts General Hospital and Harvard Medical School, Boston, MA 02114 USA, [qq]Hampton University, Hampton, VA 23668, USA, [rr]Los Alamos National Laboratory, Los Alamos, NM 87544, USA

difficult and far less sensitive than searching for it in processes where the SM Higgs boson is produced in association with a weak vector boson V (where V represents the W or Z boson). The leptonic decay of the vector boson provides a distinct signature, enabling significant suppression of QCD multijet events. Furthermore, selecting events in which jets are identified as being consistent with the fragmentation of b quarks ("b tagging") additionally improves the signal-to-background ratio in low-mass SM Higgs boson searches.

One of the most sensitive SM Higgs boson search channels at the Tevatron is the $VH \to \not\!\!E_T + b\bar{b}$ final state, where $\not\!\!E_T$ represents the missing tranverse energy resulting from neutrinos or unidentified charged leptons in the event. This article reports an update to the previous CDF analysis in the $\not\!\!E_T + b\bar{b}$ search channel [5]; the same data are analyzed, but the b-tagging strategy is significantly improved. The complete $\not\!\!E_T + b\bar{b}$ analysis method has been described previously [5] and will only be briefly reviewed. The data correspond to an integrated luminosity of 9.45 fb^{-1}, collected in proton-antiproton collisions at a center-of-mass energy of $\sqrt{s} = 1.96$ TeV.

II. CDF DETECTOR AND EVENT SELECTION

The CDF II detector is described in detail elsewhere [6, 7]. It features a cylindrical silicon detector and drift wire tracking system inside a superconducting solenoid, surrounded by projective calorimeters and muon detectors. Calorimeter energy deposits are clustered into jets using a cone algorithm with an opening angle of $\Delta R \equiv \sqrt{(\Delta\phi)^2 + (\Delta\eta)^2} = 0.4$ [8]. High-p_T electron candidates are identified by matching charged-particle tracks in the inner tracking systems [9, 10] with energy deposits in the electromagnetic calorimeters [11]. Muon candidates are identified by matching tracks with muon-detector track segments [12]. The hermeticity of the calorimeter in the pseudorapidity range $|\eta| < 2.4$ provides reliable reconstruction of the missing transverse energy [13, 14].

Events are selected during online data taking if they contain either $\not\!\!E_T(\text{cal}) > 45$ GeV, or $\not\!\!E_T(\text{cal}) > 35$ GeV and at least two jets. In the analysis, we further require that events contain no identified electron or muon, and $\not\!\!E_T > 35$ GeV after corrections for instrumental effects in jet reconstruction are applied [8]. The two jets of greatest E_T in the event are required to have transverse energies that satisfy $25 < E_T^{j_1} < 200$ GeV and $20 < E_T^{j_2} < 120$ GeV, respectively, according to a jet-energy determination based on calorimeter deposits and track momentum measurements [15]. This selects candidate events consistent with the $ZH \to \nu\bar{\nu}b\bar{b}$ process. Because τ leptons are not explicitly reconstructed and some electrons and muons escape detection or reconstruction, events from the $WH \to \ell\nu b\bar{b}$ process are also expected to contribute significantly. To gain sensitivity in events with an unidentified τ lepton, we therefore also accept events where the third-most energetic jet satisfies $15 < E_T^{j_3} < 100$ GeV. We reject events with four reconstructed jets, where each jet exceeds the minimum transverse energy threshold ($E_T > 15$ GeV) and has pseudorapidity $|\eta| < 2.4$. To reduce contamination from QCD multijet events that exhibit $\not\!\!E_T$ generated via jet mismeasurement, the angles between the $\vec{\not\!\!E}_T$ and the directions of the second and (if present) third jets are required to be greater than 0.4 radians. To ensure that both leading-E_T jets are reconstructed within the silicon detector acceptance, they are required to satisfy $|\eta| < 2$, where at least one of them must satisfy $|\eta| < 0.9$. The QCD multijet background is additionally reduced by 35% using a neural-network regression algorithm that incorporates electromagnetic- and hadronic-calorimeter quantities to account for jet-energy mismeasurements.

III. *b*-JET IDENTIFICATION ALGORITHM

This analysis employs a multivariate b-tagging algorithm (HOBIT) specifically optimized for $H \to b\bar{b}$ searches [16]. The algorithm incorporates quantities from various CDF b-tagging algorithms as input variables, and it assigns an output value v to each jet based on the probability that the jet originates from the fragmentation of a b quark. Jets initiated by b quarks tend to cluster at values close to 1, whereas those initiated by light-flavor quarks are more likely to populate the region near -1. Two operating regions are used: jets with $v \geq 0.98$ are considered to be tightly tagged (T), whereas jets with $0.72 < v < 0.98$ are loosely tagged (L). Analogous to the previous analysis, we accept events assigned to one of three categories based on the tag quality of the two leading-E_T jets: both jets are tightly tagged (TT); one jet is tightly tagged, and the other loosely tagged (TL); and only one jet is tightly tagged (1T). The tag categories used in both analyses and the associated tagging efficiencies of Higgs boson signal events are given in Table I. As can be seen, the HOBIT algorithm achieves a 32% (11%) relative improvement in the tagging efficiency of signal events into the double-tight (tight-loose) category. The

TABLE I: Comparison of b-tagging efficiencies per signal event in the tag categories of this analysis and the previous one [5]. Jets tagged by the SECVTX b-tagging algorithm are labeled "S", and those that are tagged by the JETPROB algorithm but not SECVTX are labeled "J". There is no overlap between the tag categories of a given analysis by design.

Tag category	b-tagging efficiency per event	
	Ref. [5]	This analysis
Two tight b tags	13.7% (SS)	18.1% (TT)
One tight and one loose b tag	13.1% (SJ)	14.6% (TL)
Only one tight b tag	31.4% (1S)	31.6% (1T)

preselection sample consists of events that satisfy all of the above selection criteria.

IV. QCD MULTIJET BACKGROUND MODEL

In the preselection sample, the dominant background to the Higgs boson signal is still that of QCD multijet production. Other non-neglible backgrounds are those from singly- and pair-produced top quarks ("top"), V-plus-heavy-flavor jets, diboson production (VV), and jets from electroweak processes that are incorrectly tagged as b jets ("electroweak mistags"). The modeling of each background is described in Ref. [5]. A QCD multijet background model is derived by looking at data events in a control region where $\not\!\!E_T < 70$ GeV and the angle between the $\vec{\not\!\!E}_T$ and second jet is less than 0.4 radians. The sample of events that satisfy these criteria consists almost entirely of QCD multijet contributions. For tag category i (where i = 1T, TL, or TT), a multivariable probability density function f_i is formed by taking the ratio between tagged and pretagged events as a function of several variables. Four of those variables are the same as in Ref. [5]: the scalar sum of jet transverse energies H_T, the missing track transverse momentum of the event $\not\!\!p_T$, and the charge fractions ($\sum_i p_T^i/E_T$, where the sum is over the tracks within the jet cone) of the first- and second-most energetic jets. To improve the modeling of the QCD multijet background, we include two more parameters in the probability density function: the number of reconstructed vertices in the event, which is correlated with the topological variables used in the multivariate discriminants (see Sec. V); and $p_\perp^\mu = p_{\mu 1}\sin(\hat{\boldsymbol{\mu}}_1, \hat{\mathbf{j}}_1) + p_{\mu 2}\sin(\hat{\boldsymbol{\mu}}_2, \hat{\mathbf{j}}_2)$, where $p_{\mu i}$ represents the momentum of the most energetic muon (if one exists) within the cone of jet i, and $\sin(\hat{\boldsymbol{\mu}}_i, \hat{\mathbf{j}}_i)$ is the sine of the angle between the muon and jet directions. The $p_\perp^\mu$ variable tends to be large for jets in which the initiating b quark decays semileptonically through $b \to c\ell\nu$.

A QCD multijet model is determined for each of the 1T, TL, and TT categories by weighting the untagged data in the preselection sample according to the $f_{1\mathrm{T}}$, f_{TL}, and f_{TT} probability density functions, respectively. To determine the appropriate normalization for a given category, the tagged VV, top, V-plus-heavy-flavor, and electroweak mistag background estimates are subtracted from the tagged data, and the multijet prediction is scaled to that difference. To validate the background modeling, we compare tagged data and the corresponding combined background prediction in multiple control regions [17] for various kinematic, angular, and event-shape variables, which are included later on as inputs to multivariate discriminants that separate signal and background processes. Shown in Fig. 1 are data-modeling comparisons of all tagged events in the preselection sample for the invariant dijet mass (kinematic), the angle between the $\vec{\not\!\!E}_T$ and $\vec{\not\!\!p}_T$ directions $\Delta\phi(\vec{\not\!\!E}_T, \vec{\not\!\!p}_T)$ (angular), and jet sphericity (event shape) [18] variables. The good agreement found in each distribution is representative of all variables included in the neural-network discriminants described below.

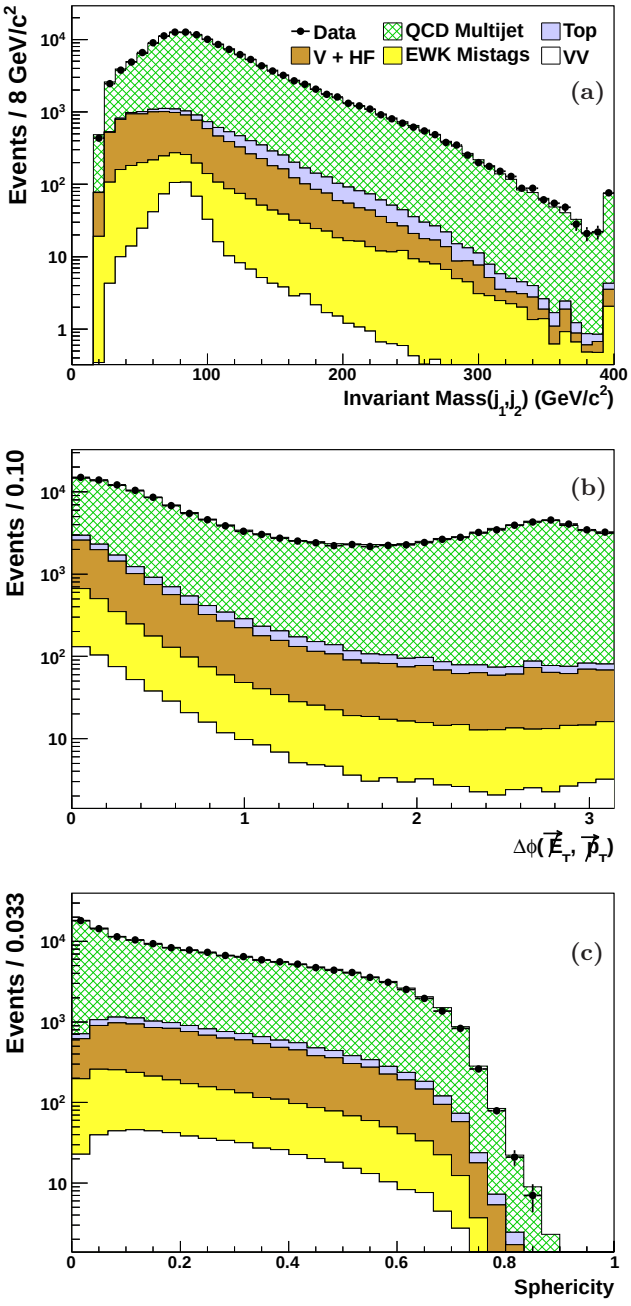

FIG. 1: Validation of the background model for all tagged events in the preselection sample for (a) the invariant mass of the two leading jets, (b) the angle between the $\vec{\not\!\!E}_T$ and $\vec{\not\!\!p}_T$, and (c) the sphericity of the jets in the event.

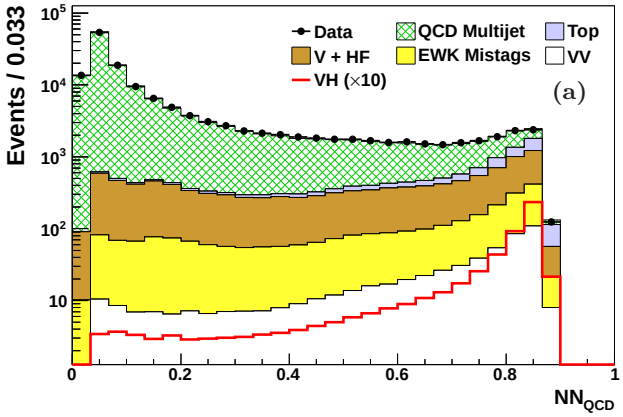

FIG. 2: The distribution of the NN_{QCD} discriminant for tagged data events in the preselection sample in comparison with modeled background expectations.

V. MULTIVARIATE DISCRIMINANTS

To optimally separate Higgs boson signal from background, a staged multivariate approach is used. A first neural network NN_{QCD} is trained to discriminate between QCD multijet and signal processes. Events that satisfy a minimum NN_{QCD} threshold requirement are subjected to a second neural network NN_{SIG}, designed to separate the signal from the remaining SM backgrounds.

The NN_{QCD} discriminant is trained using equal event yields of QCD multijet-modeled background and *VH* signal processes. As in the previous analysis, the collection of input variables to the NN_{QCD} algorithm includes kinematic, angular, and event-shape quantities [5, 19], each of which is validated with tagged data in the preselection sample. Figure 2 shows the NN_{QCD} distribution for tagged events satisfying the preselection criteria. By imposing a minimum NN_{QCD} requirement of 0.6 (which defines the *signal region*), 87% of the signal is retained while 90% of the QCD multijet background is rejected. Table II shows the expected number of signal and background events and the observed data events in the signal region. For a Higgs boson mass of 125 GeV/c^2, we expect 19 signal events in the 1T category and roughly 11 signal events in both the TL and TT categories.

Although the current and previous analyses use the same data set, the selected event samples used are only partially correlated due to updates to the *b*-tagging algorithm and the NN_{QCD} discriminant. Table III shows the predicted fractions of overlapping signal events between the tag categories of the previous analysis and those of this one. As can be seen, only 61% of the TT-tagged signal events in this analysis were present in the SS tag category of the previous analysis. The remaining 39% were classified as SJ events (23%), 1S events (11%), or were not analyzed (6%) due to either not being tagged or not surviving the minimum NN_{QCD} threshold require-

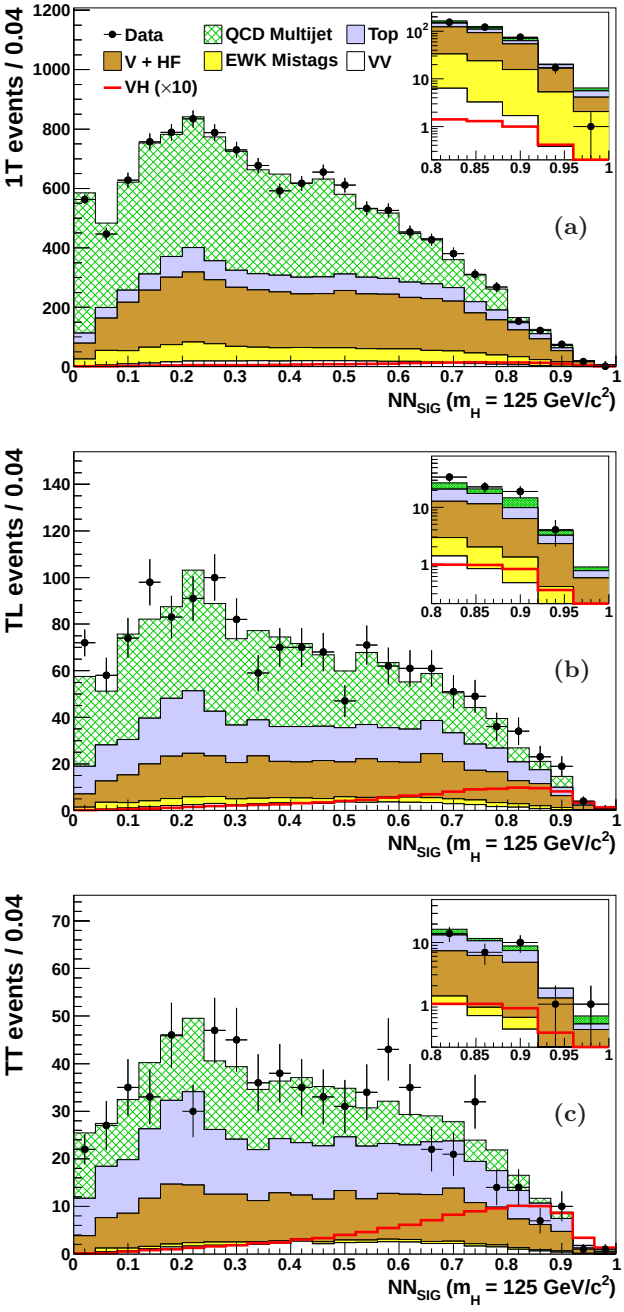

FIG. 3: The distributions of tagged data events and the corresponding expected backgrounds for the NN_{SIG} discriminant functions after fitting to data for an assumed Higgs boson mass of 125 GeV/c^2. Panel (a) shows 1T events, (b) shows TL events, and (c) shows the NN_{SIG} discriminant for TT events. The signal contribution ("*VH*") assumes a Higgs boson mass of 125 GeV/c^2 and is multiplied by a factor of ten (left unscaled in insets) for illustrative purposes. Shown in the inset is a semilogarithmic version of the same NN_{SIG} distribution for events with $NN_{SIG} > 0.8$.

TABLE II: Comparison of the number of expected and observed events in the signal region for different b-tagging categories. The uncertainties shown include systematic contributions and (when appropriate) statistical uncertainties on the simulation samples, added in quadrature for a given process. The quoted uncertainties for the total expected background prediction take into account the appropriate correlations among the systematic uncertainties for each background process. Signal contributions are given for an assumed Higgs boson mass of 125 GeV/c^2.

Process	1T	TL	TT
QCD multijet	5941 ± 178	637 ± 25	222 ± 16
Top	1174 ± 158	302 ± 40	271 ± 34
V + heavy flavor jets	3124 ± 718	286 ± 83	211 ± 65
Electroweak mistags	1070 ± 386	55 ± 21	13 ± 6
Diboson	305 ± 46	48 ± 6	41 ± 5
Total expected background	11612 ± 949	1329 ± 112	759 ± 86
Observed data	11955	1443	692
$ZH \to \nu\bar{\nu}b\bar{b}, \ell\ell b\bar{b}$	9.7 ± 1.0	5.4 ± 0.5	5.4 ± 0.5
$WH \to \ell\nu b\bar{b}$	9.8 ± 1.0	5.3 ± 0.5	5.3 ± 0.5

TABLE III: Predicted fractions of overlapping signal events between the previous analysis and this one. The "0T/0S" categories represent events that do not survive the tagging or signal-region definition criteria. Roman-font (italicized) numbers represent percentages of overlapping events relative to this (the previous) analysis [5]; the sum of the percentages in each column (row) is 100%. A Higgs boson mass of 125 GeV/c^2 is assumed.

	0T		1T		TL		TT	
0S			—	22%	—	19%	—	6%
1S	*17%*	—	*63%*	67%	*15%*	31%	*6%*	11%
SJ	*12%*	—	*20%*	9%	*37%*	35%	*32%*	23%
SS	*5%*	—	*3%*	1%	*15%*	15%	*77%*	61%

ment. A significant portion of TT signal events is therefore different from the sample of SS events in the previous analysis. The percentage of TT data events in this analysis also present in the SS category of the previous one is approximately 50%.

The $\mathrm{NN_{SIG}}$ discriminant functions trained in the previous analysis [5] are well modeled in the analogous HOBIT categories and also provide good separation of signal and background events; they were thus retained for this analysis. The $\mathrm{NN_{SIG}}$ discriminant accepts kinematic and angular quantities as input variables, as well as the $\mathrm{NN_{QCD}}$ value and a neural-network output that attempts to disentangle intrinsic $\not\!\!E_T$ from instrumental $\not\!\!E_T$ by using tracking information [19]. The modeling of each input variable is validated with tagged data in the signal region. Figure 3 shows the $\mathrm{NN_{SIG}}$ distribution in the signal region ($\mathrm{NN_{QCD}} > 0.6$) for the 1T, TL, and TT events after the discriminants from all tag categories were jointly fitted to data.

VI. RESULTS

We perform a binned likelihood fit to search for the presence of a Higgs boson signal. A combined likelihood is formed from the product of Poisson probabilities of the event yield in each bin of the $\mathrm{NN_{SIG}}$ distribution for each tag category. Systematic uncertainties are treated as nuisance parameters and incorporated into the limit by assuming Gaussian prior probabilities, centered at the nominal value of the nuisance parameter, with an RMS width equal to the absolute value of the uncertainty. The dominant systematic uncertainties arise from the normalization of the V-plus-heavy-flavor background contributions (30%), differences in b-tagging efficiencies between data and simulation (8–16%) [16], uncertainty on the top (6.5–10%) and diboson (6%) cross sections [20, 21], normalizations of the QCD multijet background (3–7%), luminosity determination (6%) [22], jet-energy scale (6%) [8], trigger efficiency (1–3%), parton distribution functions (2%), and lepton vetoes (2%). Additional uncertainties applied only to signal include those on the Higgs boson production cross section (5%) [23] and on initial- and final-state radiation effects (2%). Also included are uncertainties in the $\mathrm{NN_{SIG}}$ shape, which arise primarily from variations in the jet-energy scale and the QCD multijet background model.

A Bayesian likelihood method is used to set 95% credibility level (C.L.) upper limits on the SM Higgs boson production cross section times branching fraction $\sigma(VH) \times \mathcal{B}(H \to b\bar{b})$. For the signal hypothesis, a flat, non-negative prior probability is assumed for the number of selected Higgs boson events. The Gaussian priors of the nuisance parameters are truncated at zero to ensure non-negative event yield predictions in each $\mathrm{NN_{SIG}}$ bin. The 95% C.L. limits for the observed data and the median-expected outcomes assuming only SM backgrounds are shown in Fig. 4 and Table IV. An average

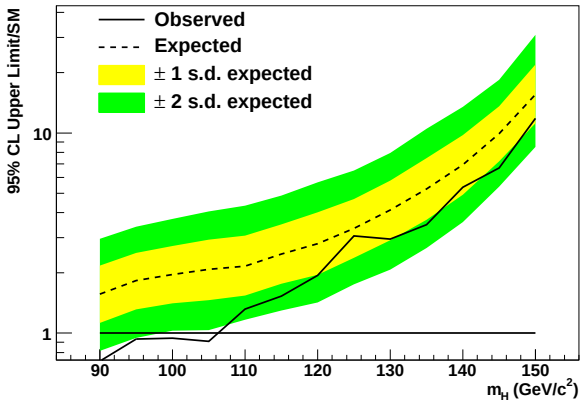

FIG. 4: Observed and expected (median, for the background-only hypothesis) 95% C.L. upper limits on VH cross section times $\mathcal{B}(H \to b\bar{b})$ divided by the SM prediction, as a function of the Higgs boson mass. The bands indicate the 68% and 95% credibility regions where the limits can fluctuate, in the absence of signal.

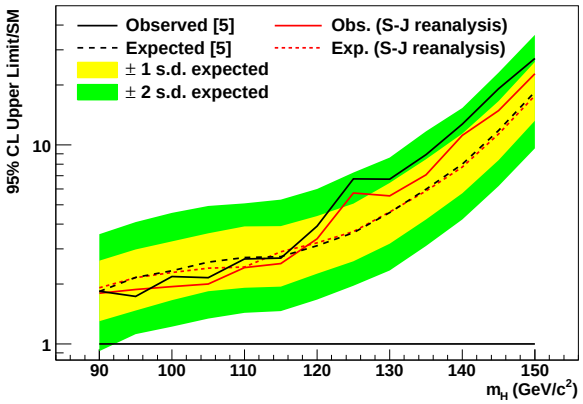

FIG. 5: Observed and expected (median, for the background-only hypothesis) 95% C.L. upper limits on Higgs production in the previous analysis [5] and those of the S-J reanalysis described in Sec. VII A. The darker (black) set of lines represent the observed and expected limits from the previous analysis, whereas the lighter set (red) represent those of the S-J reanalysis. The 68% and 95% credibility regions are those of Ref. [5].

improvement of 14% is obtained in expected upper limits relative to the previous analysis [5]. The observed limits lie below the expected values at the level of roughly one standard deviation for $m_H \geq 120$ GeV/c^2, and at the level of approximately two standard deviations for lower Higgs boson masses. In constrast, the observed limits of the previous analysis exceed the median-expected limits by roughly one standard deviation for $m_H > 120$ GeV/c^2 and are in approximate agreement with expected limits for lower masses. These differences correspond to a decrease of roughly 55% in the observed limits relative to those of the previous analysis [5] independent of m_H.

VII. DISCUSSION OF RESULTS

We have investigated potential causes for the sizable shift in the observed limits. To quantify the impact of changes to the analysis design and treatment of systematic uncertainties, we reanalyze the data sample using the 1S, SJ, and SS categories used in the previous analysis (Sec. VII A). We also study the effects from other sources that can influence the observed limits (Sec. VII B). A summary of the discussion is given in Sec. VII C.

A. Reanalysis using 1S, SJ, and SS tagging categories

Besides the change in b-tagging method, there are other less significant changes made in this analysis with respect to the previous one:

1. The b-tag scale factors and their associated uncertainties are now handled with an improved treatment of the correlations between tag categories.

2. Instead of treating the normalization uncertainties of all V-plus-heavy-flavor samples as fully correlated, the V-plus-heavy-flavor samples are grouped according to flavor content of the final state, with each group receiving a 30% uncertainty. The uncertainties associated with each V-plus-heavy-flavor group are treated as uncorrelated with one another.

3. An additional $\not\!\!E_T > 35$ GeV requirement is made that corresponds to the trigger-level reconstructed $\not\!\!E_T$ value. This has the effect of further reducing the QCD multijet background at the few percent level.

4. As mentioned in Sec. II, upper limits are imposed on jet transverse energies. This is done to avoid a kinematic region susceptible to significant false-positive tagging rates for the HOBIT algorithm.

5. An additional Z-plus-jets sample is included where the Z boson decays to a $b\bar{b}$ pair. The change in overall expected yields due to this additional sample is very small as the $\not\!\!E_T$ here is instrumental.

To estimate the effect of these changes on the limits, we reanalyze the same data sample using the 1S, SJ, and SS tagging categories of the previous analysis. For this test, hereafter referred to as the *S-J reanalysis*, we retain the $\mathrm{NN_{QCD}}$ discriminant of the previous analysis so that the signal region definitions of this test and that of the previous analysis are the same. The results are shown in Fig. 5. As can be seen, the expected limits of Ref. [5] and the S-J reanalysis are in very good agreement. The observed limits of the S-J reanalysis are systematically lower than the observed limits of Ref. [5]

TABLE IV: Expected and observed 95% C.L. upper limits on the VH cross section times $\mathcal{B}(H \to b\bar{b})$ divided by the SM prediction [24].

m_H (GeV/c^2)	90	95	100	105	110	115	120	125	130	135	140	145	150
Expected	1.57	1.83	1.96	2.08	2.16	2.48	2.80	3.33	4.13	5.26	6.93	9.91	15.55
Observed	0.72	0.94	0.94	0.91	1.32	1.53	1.94	3.06	2.95	3.49	5.35	6.69	11.82

with an average difference of -5% for $m_H < 120$ GeV/c^2 and -17% for $m_H \geq 120$ GeV/c^2. For comparison, we note that the observed limit for the analysis described in this note is 47% lower than that of the S-J reanalysis at $m_H = 125$ GeV/c^2. The analysis changes described here thus account for a non-negligible percentage of the sizable shift in the observed limits.

We have also investigated the impact of these changes on previously published combined CDF $H \to b\bar{b}$ limits [25]. The $\mathrm{NN_{SIG}}$ discriminants of the S-J reanalysis, and the updated treatment of systematic uncertainties, are combined with the discriminants of the CDF $\ell\nu b\bar{b}$ and $\ell\ell b\bar{b}$ analyses [26, 27] to obtain an updated CDF $H \to b\bar{b}$ result. Using the discriminants of the S-J reanalysis, the local significance of the CDF-combined excess at a Higgs boson mass of 125 GeV/c^2 is recalculated. Within the statistical precision of the calculation, the local significance is unchanged at 2.7 standard deviations with respect to the background-only hypothesis.

B. Additional cross-checks

1. *Systematic effects from b-tagging*

Since switching to a new b-tagging algorithm is the most significant change adopted for this analysis, it is important to ensure that the performance of the HOBIT algorithm is well understood and well modeled. As with other b-tagging algorithms, systematic effects associated with using HOBIT are taken into account by correcting the simulation for differences in b-tagging behavior between data and simulation. Two methods are used to calibrate the simulation, both of which have been used extensively at CDF: one where the $t\bar{t}$ cross section is fixed to its theoretical prediction, and scale factors are derived that correct the simulation to the b-tag and mistag efficiencies measured in data; and another where heavy- and light-flavor jets are identified with and without electron conversions within them, allowing for a determination of the same scale factors [16]. As both methods give consistent results for the HOBIT scale factors at both T and L operating points, they are averaged together, resulting in b-tag efficiency scale factors of 0.915 ± 0.035 (T) and 0.993 ± 0.035 (L) and mistag efficiency scale factors of 1.50 ± 0.031 (T) and 1.33 ± 0.015 (L), where the dominant contributions to the uncertainties are from the theoretical uncertainty on the $t\bar{t}$ cross section [28]. The variation of these scale factors with respect to several variables (e.g., jet energies and instantaneous luminosity) has been investigated, and any sizable deviations relative to the central predictions are included in the systematic uncertainties. These scale factors and their associated uncertainties have been propagated through this analysis in a manner consistent with the treatment of b-tag and mistag scale factors in the other $H \to b\bar{b}$ CDF analyses [26, 27].

To verify that the choice of b-tagging algorithm does not result in mismodeling within the high-score regions of the $\mathrm{NN_{SIG}}$ distributions, we validate the background model with the data in an *electroweak control sample*. For this control sample we require, in addition to the preselection sample criteria, the presence of at least one identified, isolated electron or muon with a minimum transverse momentum of 20 GeV/c in the event. The electroweak sample is dominated by backgrounds that are modeled by simulation and not the QCD multijet background, whose model is derived from data. Figure 6 shows the $\mathrm{NN_{SIG}}$ distributions for TT and reanalyzed SS events in the electroweak control region. As can be seen, there is no obvious difference in the simulation modeling of the $\mathrm{NN_{SIG}}$ discriminants for the HOBIT or SECVTX algorithms. Comparisons in the 1T-1S and TL-SJ categories give similar conclusions.

2. *Effects of statistical fluctuations*

The expected limits are most significantly impacted by the bins of the discriminants with the highest signal-to-background ratios. For the $\mathrm{NN_{SIG}}$ distributions, these are the bins with the highest $\mathrm{NN_{SIG}}$ values, as can be seen in Fig. 3. Because these bins tend to contain only small numbers of data events, the observed limits are susceptible to statistical fluctuations. Although we do not know if the data events are from signal or background processes, we explore how a fluctuation of yields from either type of process would manifest itself in the $\mathrm{NN_{SIG}}$ distributions. As part of the shift in observed limits is due to the analysis changes mentioned in Sec. VII A, the yields quoted below for the SS and SJ results reflect those of the S-J reanalysis and not those of Ref. [5].

As shown in Table III, we expect significant signal event migrations between the tag categories of the previous analysis and those of this one. Consequently, if a Higgs boson signal is present, we may observe some very high $\mathrm{NN_{SIG}}$ score events in one version of the analysis that either migrate to another tag category or do not ap-

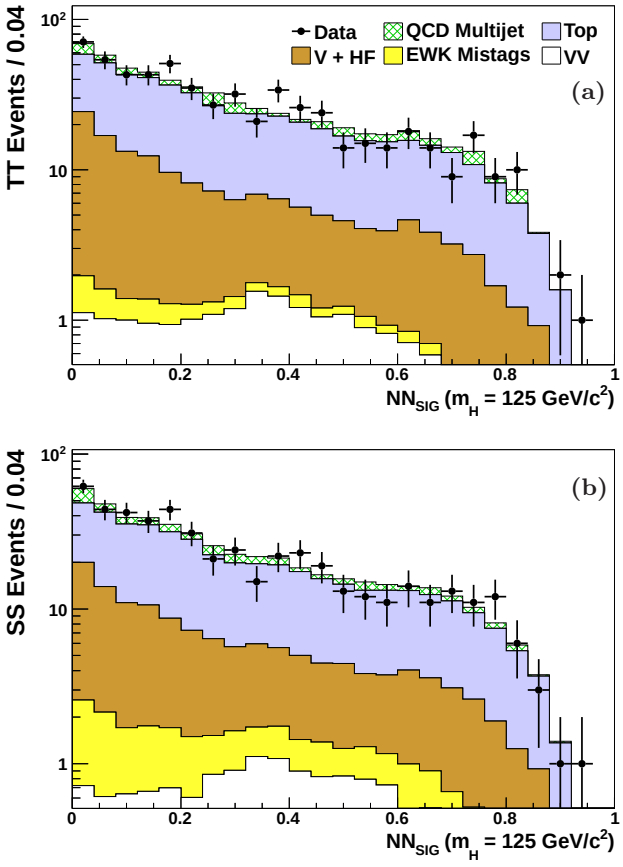

FIG. 6: Validation of the background model for (a) TT events and (b) reanalyzed SS events in the electroweak control region.

pear within the other analysis. Since the impact of these high-score events on the observed limits can be significant, the migration of a few signal-like events between tag categories in the S-J reanalysis and the current analysis can lead to non-negligible changes in observed limits relative to expectations. Focusing on discriminant outputs for the 125 GeV/c^2 Higgs boson mass hypothesis, we compare data events in the very highest-score $\mathrm{NN_{SIG}}$ bins of both analyses and find one potential example for this type of event migration. In particular, we observe three events with $\mathrm{NN_{SIG}}$ values above 0.9 in the SJ category that are not present in any tag category of the current analysis (the new tagging algorithm categorizes two of these events as LL and the other as 1L). If these three data events were to be simply added back into the TL category of the new analysis, the decrease in the observed limits at $m_H = 125$ GeV/c^2 with respect to those of the S-J reanalysis would be reduced from 47% to 31%.

The number of expected background events in the high-score region of the $\mathrm{NN_{SIG}}$ discrimimants is also small and therefore an additional source of potential statistical fluctuations in the data that might significantly impact the observed limits. We check for a potential

TABLE V: Percentages of overlapping events between tag categories of this analysis and the previous one for data events with $\mathrm{NN_{SIG}}$ values greater than 0.8.

	1T	TL	TT
1S	55%	35%	15%
SJ	4%	20%	30%
SS	1%	14%	51%

effect from background event fluctuations on the difference between observed limits of the $m_H = 125$ GeV/c^2 searches by comparing the number of observed events that satisfy $\mathrm{NN_{SIG}} > 0.8$ to the fitted background predictions for each tag category in the current analysis and the S-J reanalysis. For the most sensitive double-tag categories, the predicted (observed) event yields in the high-score $\mathrm{NN_{SIG}}$ region are 37.6 ± 4.6 (37) for SS and 45.6 ± 5.1 (62) for SJ and 39.5 ± 4.6 (33) for TT and 67.4 ± 6.8 (80) for TL. While the SJ and TL categories exhibit similar upward fluctuations in data relative to expectations, the data in the SS (TT) category are consistent with (lower than) the background expectation.

A simple test is performed in which 5 data events are added into the high-score region of the TT $\mathrm{NN_{SIG}}$ distribution (maintaining the relative fractions of observed events within each high-score bin) to approximately match the expected background, as was observed in the SS category. This change reduces the difference between the present and S-J reanalyzed limits to 33%. Combining this effect with that of adding the 3 formerly SJ-classified events into the TL category gives a decrease in observed limits of 19% relative to the S-J analysis. This is in reasonable agreement with the expected improvement, identifying these two effects in data as the primary source of the change in observed limits at $m_H = 125$ GeV/c^2.

To estimate the probability of an underlying statistical effect causing such a sizable change in observed limits, correlations between the event samples must be understood. For technical reasons we are not able to determine these correlations separately for each background process. Instead, we look directly at the data in the high-score regions of the $\mathrm{NN_{SIG}}$ discriminants, and calculate the percentage overlap between the tag categories of this analysis and those of the S-J reanalysis. The overlap percentages, relative to the current analysis, are given in Table V. Based on these percentages, we use simulated data experiments to estimate the probability that the observed limits of this analysis and the S-J reanalysis are compatible. Figure 7 shows a two-dimensional distribution of expected upper limits, obtained from producing pairs of expected outcomes between the HOBIT analysis and S-J reanalysis. To calculate a compatibility probability (p-value), the probability is estimated for the HOBIT analysis to be as or more discrepant that what is observed, given the observed limit of the S-J reanalysis.

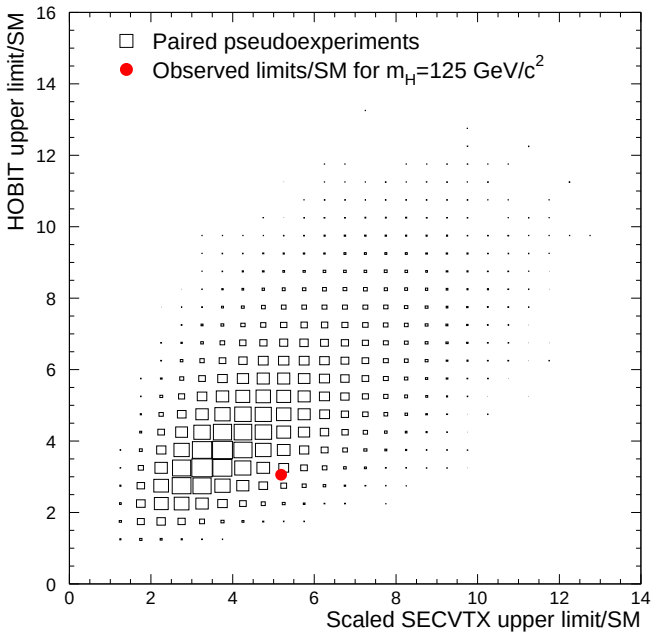

FIG. 7: Pseudoexperiment pairs of expected 95% C.L. upper limits on Higgs production assuming the HOBIT analysis (ordinate) and S-J reanalysis (abscissa). For ease in p-value computation, the expected limits of the S-J reanalysis are rescaled such that the median-expected limit agrees with that of the HOBIT analysis.

The two-sided probability for this type of occurrence at a Higgs boson mass of 125 GeV/c^2 is roughly 7%.

As a downward shift in observed limits is seen across the entire range of tested m_H values and not just at $m_H = 125$ GeV/c^2, the probability for such a global shift to occur must be estimated. Limited experimental resolution of kinematic event input variables to the multivariate discriminants leads to events being shared within the high-score $\mathrm{NN_{SIG}}$ regions of the outputs for neighboring mass hypotheses. Because of this, we estimate that the number of independent search regions within our tested Higgs boson mass range lies somewhere between two and three. We therefore perform the pseudoexperiment study for three Higgs boson mass assumptions, obtaining p-values at $m_H = 100$, 125 and 150 GeV/c^2. Each p-value is on the order of 10%. To estimate an approximate global probability, we combine the obtained p-values for the three Higgs boson mass assumptions using Fisher's method for combining independent tests. We obtain a global probability of roughly 3% or 5% depending on whether the number of independent kinematic search regions is three or two, respectively.

3. Background modeling

In order to conclude that the observed effect in data originates from statistical fluctuations as opposed to potential background mismodeling, we confirm the robustness of our background model in several data control samples. Events in the intermediate-score region of the $\mathrm{NN_{SIG}}$ distributions are also useful for testing the background modeling. We compare predicted and observed event yields in the $\mathrm{NN_{SIG}}$ score region between 0.5 and 0.8, which contains higher event yields but is above the low-score event region, which drives the fitted normalizations of the background contributions. Assuming a Higgs boson mass of 125 GeV/c^2, the predicted (observed) event yields in the intermediate score $\mathrm{NN_{SIG}}$ region are 228.8±21.0 (217) for SS and 312.5±22.6 (291) for SJ in the S-J reanalysis and 264.8±25.1 (265) for TT and 506.1±38.8 (506) for TL in the current one. Good agreement between the observed and predicted event yields is found at the other Higgs boson mass assumptions as well. In the intermediate-score regions, there is thus no indication of a background modeling problem that could account for such sizable shifts in observed limits with respect to the S-J reanalysis.

C. Summary of discussion

To summarize, the observed limits are very sensitive to statistical fluctuations in the highest-value bins of the $\mathrm{NN_{SIG}}$ distributions. There is no evidence of any significant mismodeling of the HOBIT b-jet identification algorithm, or of the $\mathrm{NN_{QCD}}$ or $\mathrm{NN_{SIG}}$ distributions and the distributions of their respective input variables in any of the control regions studied. The observed migration of events across the b-tag categories is fairly consistent with expectations derived from simulation. In the most sensitive tag category, TT, the data yield is about 1 standard deviation below the background prediction in the signal region. Using an ensemble of simulated experiments, we estimate the probability that the observed limit could change, relative to the S-J reanalysis, by an amount at least as large as that observed due to statistical fluctuations alone is about 5%. We conclude that the change in the observed limits relative to the previous analysis is primarily due to statistical fluctuations.

VIII. CONCLUSION

In conclusion, we have performed an updated Higgs boson search in the $\not\!\!E_T + b\bar{b}$ final state, using the full CDF data set and an improved b-tagging algorithm. With respect to the previous analysis [5], the expected 95% C.L. limits have improved by 14% on average across the Higgs boson mass range $90 \leq m_H \leq 150$ GeV/c^2. The 95% observed upper limit at a Higgs boson mass of 125 GeV/c^2 is a factor of 3.06 times the SM prediction. The results of this analysis correspond to some of the most sensitive limits obtained on Higgs boson production in the $b\bar{b}$ final state.

IX. ACKNOWLEDGMENTS

We thank the Fermilab staff and the technical staffs of the participating institutions for their vital contributions. This work was supported by the U.S. Department of Energy and National Science Foundation; the Italian Istituto Nazionale di Fisica Nucleare; the Ministry of Education, Culture, Sports, Science and Technology of Japan; the Natural Sciences and Engineering Research Council of Canada; the National Science Council of the Republic of China; the Swiss National Science Foundation; the A.P. Sloan Foundation; the Bundesministerium für Bildung und Forschung, Germany; the Korean World Class University Program, the National Research Foundation of Korea; the Science and Technology Facilities Council and the Royal Society, UK; the Russian Foundation for Basic Research; the Ministerio de Ciencia e Innovación, and Programa Consolider-Ingenio 2010, Spain; the Slovak R&D Agency; the Academy of Finland; the Australian Research Council (ARC); and the EU community Marie Curie Fellowship contract 302103.

[1] S. Glashow, Nucl. Phys. **22**, 579 (1961); S. Weinberg, Phys. Rev. Lett. **19**, 1264 (1967); A. Salam, *Elementary Particle Theory*, ed. N. Svartholm (Almqvist and Wiksell, Stockholm), 367 (1968).

[2] F. Englert and R. Brout, Phys. Rev. Lett. **13**, 321 (1964); P. W. Higgs, Phys. Rev. Lett. **13**, 508 (1964); G. S. Guralnik, C. R. Hagen, and T. W. B. Kibble, Phys. Rev. Lett. **13**, 585 (1964).

[3] S. Chatrchyan *et al.* (CMS Collaboration), Phys. Lett. B **716**, 30 (2012); G. Aad *et al.* (ATLAS Collaboration), Phys. Lett. B **716**, 1 (2012).

[4] T. Aaltonen *et al.* (CDF Collaboration, D0 Collaboration), Phys. Rev. Lett. **109**, 071804 (2012).

[5] T. Aaltonen *et al.* (CDF Collaboration), Phys. Rev. Lett. **109**, 111805 (2012).

[6] D. Acosta *et al.* (CDF Collaboration), Phys. Rev. D **71**, 032001 (2005); D. Acosta *et al.* (CDF Collaboration), Phys. Rev. D **71**, 052003 (2005); A. Abulencia *et al.* (CDF Collaboration), J. Phys. G Nucl. Part. Phys. **34**, 2457 (2007).

[7] We use a cylindrical coordinate system with the origin at the center of the CDF detector, z pointing in the direction of the proton beam, θ and ϕ representing the polar and azimuthal angles, respectively, and pseudorapidity defined by $\eta = -\ln \tan(\theta/2)$. The transverse momentum p_T (transverse energy E_T) is defined to be $p \sin\theta$ ($E \sin\theta$).

[8] A. Bhatti *et al.*, Nucl. Instrum. Methods Phys. Res., Sect. A **566**, 375 (2006).

[9] A. Sill *et al.*, Nucl. Instrum. Methods Phys. Res., Sect. A **447**, 1 (2000); A. Affolder *et al.*, Nucl. Instrum. Methods Phys. Res., Sect. A **453**, 84 (2000); C. S. Hill *et al.*, Nucl. Instrum. Methods Phys. Res., Sect. A **511**, 118 (2003).

[10] A. Affolder *et al.*, Nucl. Instrum. Methods Phys. Res., Sect. A **526**, 249 (2004).

[11] L. Balka *et al.*, Nucl. Instrum. Methods Phys. Res., Sect. A **267**, 272 (1988); M. G. Albrow *et al.*, Nucl. Instrum. Methods Phys. Res., Sect. A **480**, 524 (2002).

[12] G. Ascoli *et al.*, Nucl. Instrum. Methods Phys. Res., Sect. A **268**, 33 (1988).

[13] The calorimeter missing transverse energy $\vec{\not\!\!E}_T$(cal) is defined by the sum over calorimeter towers, $\vec{\not\!\!E}_T(\text{cal}) = -\sum_i E_T^i \hat{n}_i$, where i is a calorimeter tower number with $|\eta| < 3.6$, $\hat{n}_i$ is a unit vector perpendicular to the beam axis and pointing at the ith calorimeter tower. The reconstructed missing transverse energy, $\vec{\not\!\!E}_T$, is derived by subtracting from $\vec{\not\!\!E}_T$(cal) components of the event not registered by the calorimeter, such as jet energy adjustments. $\not\!\!E_T$ [$\not\!\!E_T$(cal)] is the scalar magnitude of $\vec{\not\!\!E}_T$ [$\vec{\not\!\!E}_T$(cal)].

[14] S. Bertolucci *et al.*, Nucl. Instrum. Methods Phys. Res., Sect. A **267**, 301 (1988).

[15] C. Adloff *et al.* (H1 Collaboration), Z. Phys. C **74**, 221 (1997).

[16] J. Freeman, T. Junk, M. Kirby, Y. Oksuzian, T. J. Phillips, F. D. Snider, M. Trovato, J. Vizan, and W. M. Yao, Nucl. Instrum. Methods Phys. Res., Sect. A **697**, 64 (2013).

[17] We validate the background model by comparing with tagged data events in the preselection sample, the electroweak control sample (Sec. VII B 1) and also in the MJ1, MJ2, and MJ3 control regions as defined in Ref. [5].

[18] The jet sphericity is defined as $S = \frac{3}{2}(\lambda_2 + \lambda_3)$, where $\lambda_{2,3}$ are eigenvalues of the sphericity tensor $S^{\alpha\beta} = \sum_i p_i^\alpha p_i^\beta / \sum_i p_i^2$, with the sums extending over each jet i with transverse energy greater than 15 GeV. The eigenvalues are ranked according to $\lambda_1 > \lambda_2 > \lambda_3$, and they satisfy $\lambda_1 + \lambda_2 + \lambda_3 = 1$.

[19] K. Potamianos, Ph.D. thesis, Purdue University, FERMILAB-THESIS-2011-34.

[20] S. Moch and P. Uwer, Nucl. Phys. B, Proc. Suppl. **183**, 75 (2008); N. Kidonakis, Phys. Rev. D **74**, 114012 (2006).

[21] J. M. Campbell and R. K. Ellis, Phys. Rev. D **60**, 113006 (1999).

[22] S. Klimenko, J. Konigsberg, and T. M. Liss, Report No. FERMILAB-FN-0741, 2003.

[23] J. Baglio and A. Djouadi, J. High Energy Phys. 10 (2010) 064; O. Brien, R. V. Harlander, M. Weisemann, and T. Zirke, Eur. Phys. J. C **72**, 1868 (2012).

[24] The CDF and D0 Collaborations and the Tevatron New Physics and Higgs Working Group, arXiv:1207.0449v2.

[25] T. Aaltonen *et al.* (CDF Collaboration), Phys. Rev. Lett. **109**, 111802 (2012).

[26] T. Aaltonen *et al.* (CDF Collaboration), Phys. Rev. Lett. **109**, 111804 (2012).

[27] T. Aaltonen *et al.* (CDF Collaboration), Phys. Rev. Lett. **109**, 111803 (2012).

[28] U. Langenfeld, S. Moch, and P. Uwer, Phys. Rev. D **80**, 054009 (2009).